CHAPTER-4

Facile One-Pot Synthesis of ZnO Nanoparticles on reduced Graphene Oxide nanosheet (ZnONPs@rGO) As a proficient heterogeneous catalyst for multicomponent A^3-coupling

[4.1] Introduction

The Nitrogen-based heterocyclic compounds have huge potential to be employed in wide range of applications such as their pharmaceutical and biological activities. The formation of Nitrogen-based heterocyclic compounds via A^3-coupling reaction involves the reaction between an aldehyde, β-keto ester, and urea or thio-urea is now-a-days one of the most fascinated coupling reactions that used to produce dihydropyrimidinones (DHPMs). Additionally, these reactions are mild, low-cost and one-pot (in situ) synthesis. The product dihydropyrimidinones (DHPMs) has received a much attention owing to the discovery of the calcium channel modulating drug, Nifedipine, containing the DHPM backbone, utilizing for the treatment of cardiovascular disease. The discovery of monastrol containing DHPMs compound was found effectual as an anticancer agent for inhibiting mitotic kinesin Eg5. Furthermore, DHPMs compounds viz. SQ 32547 and SWO_2 are found pertinent as a useful orally active antihypertensive agent. On the other hand, several esters and cyanide containing DHPMs are found suitable as antibacterial agents. [1-6]

In recent decades, the A^3- coupling reaction has been performed over strong acidic catalysts such as $TiCl_3$, $BF_3.OEt_2$, $ZrCl_4$, $InBr_3$, $BiCl_3$, Me_3SiCl, LiBr, $Mn(OAc)_3.2H_2O$, $La(OTf)_3$, $Yb(OTf)_3$, and $Sc(OTf)_3$. All of the aforesaid systems have been proposed to demonstrate more or less highly active and -selective products due to the presence of easily accessible active sites. [7-20] However, these systems are often regarded as imprecise with many impediments, including agglomeration of active sites; the contamination of toxic metal is also found along with the product which is comparatively detrimental one when dealing with the synthesis of biological products. In this regard, the non-recoverable catalyst from the product is the key challenging task in the research field. Therefore, to get rid out of these problems and minimize hazards in biological products, the solid supported catalysts have been widely preferred. In addition to this, the need for the solid supported catalysts is caused by the presence of large surface area, defects sites and excellent mechanical strength in relation to the total catalyst loading, which helps to easily adsorbed of the more

active site i.e. active metal precursor. At the present time, the effective and multifaceted solid supports such as silica, activated carbon, zeolites, SBA-15 and several others have been reported for one-pot coupling reaction including Homo coupling, cross-coupling and A^3-coupling reactions [20-25]. Previously, Fe_3O_4 nanoparticles embedded on the mesoporous SBA-15 support using an "in situ" approach have been reported by D. Bhuyan and co-workers [26] and catalytically tested over A^3-coupling reaction. Bao-Dui Wang et al. [27] have been synthesized graphene-Fe_3O_4 catalyst with unwavering Fe_3O_4 NPs by the decomposition of $Fe(CO)_5$ on the surface of graphene oxide. The uniqueness of this work is that the decomposition products of $Fe(CO)_5$ retaliated with GO leading to the formation of graphene-Fe_3O_4. The resulting catalyst was tested over A^3-coupling reaction. Another work based on manganese-containing periodic mesoporous organosilica with ionic-liquid framework (Mn@PMO/IL) in the A^3-coupling reaction was investigated by D. Elhamifar and co-workers. [28]

Transition metal oxide shows enormous prospective in many important organic transformations due to their controlled shape, size, stability, a non toxic, crystallinity and functionality, corrosion resistance, easily scalable, relatively cost effective and non-hygroscopic property, making it as a proficient catalyst. In past few decades, rGO/ZnO nanocomposites have been explored in various fields such as electrochemical capacitors, [29] adsorbents for pollutants and removal of RhB dye from water, [30] photocatalysts and manufacture of organic photovoltaics [31]. Though for organic transformations, [32-33] ZnO nanoparticles (NPs) have been established as solitary heterogeneous catalysts however, to the best of our knowledge, only few reports on rGO/ZnO nanocomposites as catalysts have been reported in the literature [34-36]. Here in this chapter, we report A^3-coupling reaction (via 'one-pot' method) catalyzed by ZnONPs@rGO. In this nanocomposite, ZnO nanoparticles (NPs) are uniformly dispersed on the rGO nanosheet, which actually prevents the aggregation of ZnONPs. The other salient feature of rGO nanosheet as a support is the presence of defected sites which can allow the substrate molecule to be easily anchored over the active site.

[4.2] Experimental Section

(a) Materials

Natural flake graphite (325 mesh, 99.95%) was purchased from Sigma Aldrich. potassium permanganate, zinc acetate was acquired from MERCK India Pvt Ltd. Urea, ethyl acetoacetate, methyl acetoacetate, sulphuric acid, sodium nitrate, l-ascorbic acid, hydrochloric acid, 30% hydrogen peroxide, benzaldehyde, 4-methyl benzaldehyde, 4-methoxy benzaldehyde, furfuraldehyde, 4-nitro benzaldehyde were procured from S D Fine Chem Ltd. All the materials are of analytical grade and used as received without further purification.

(b) Synthesis of graphene oxide (GO)

Graphene oxide was synthesized from graphite flakes using a modified Hummer's method [37].

(c) Synthesis of ZnO nanoparticles (ZnONPs)

The ZnONPs were prepared as follows: Zinc acetate dehydrate 2 g) was dissolved in 20 mL of deionized water. This aqueous solution of zinc acetate was then heated at 70 ℃ with continuous stirring in a magnetic stirrer. Then, a freshly prepared (4 g) NaOH solution was added drop wise into an aqueous solution of zinc acetate with constant stirring and refluxed for 4 h at 70 ℃. The obtained white suspension was filtered, carefully washed with deionized water (until the pH maintained up to 6), dried in air oven at 70 °C and finally calcined at 550 °C for 6 h to get white powder of ZnO nanoparticles.

$$Zn(CH3COO)_2 + NaOH \rightarrow Zn(OH)_2 + 2CH_3COONa;$$

$$Zn(OH)_2 \rightarrow ZnO + H_2O$$

(d) Synthesis of ZnONPs@rGO nanocatalyst

A 50 mg of GO was dispersed into deionized water (15 mL) in a 250 mL beaker followed by a dropwise addition of 10 mmol $Zn(CH_3COO)_2$ solution and then ultrasonicated for 20 min to produce uniformly dispersed suspension. A freshly prepared solution of l-ascorbic acid (25 mL) was then added drop wise into the above suspension with constant stirring and heated at 90 ℃ for 4 h. The obtained black precipitates signify the successful reduction of both metal salts and

GO. The excess of ascorbic acid can be eradicated from the product using H_2O_2 solution. The solid product was separated by centrifugation followed by washed with ethanol and deionized water and finally dried in an oven at 65 ^oC.

(e) Catalytic test

In a typical Biginelli reaction experiment, a mixture of 1 mmol of benzaldehyde, 1 mmol of ethyl acetoacetate, 0.8 mmol of urea, 5 mL solvent and 10 mg catalyst were added into a 50 mL round bottom flask and the reaction mixture was kept under vigorous stirring. The reaction progress was screened by TLC. The reaction mixture was filtered; the solvent was evaporated from the filtrate under reduced pressure to achieve a solid product. However, Separation was carried out by column chromatography over silica gel using petroleum ether and ethyl acetate as an eluent. The pure product was characterized by ^1H NMR spectral analysis, melting point and compared with reported data.

[4.3] Results and discussion

The aforesaid synthesized ZnONPs@rGO nanocatalyst was thoroughly corroborated by various physico-chemical techniques such as FT-IR, Raman, XRD, XPS, HR-TEM, and thermogravimetric analysis. The results of as-prepared nanocatalysts have been discussed in this section as follows:

(a) Raman spectra:

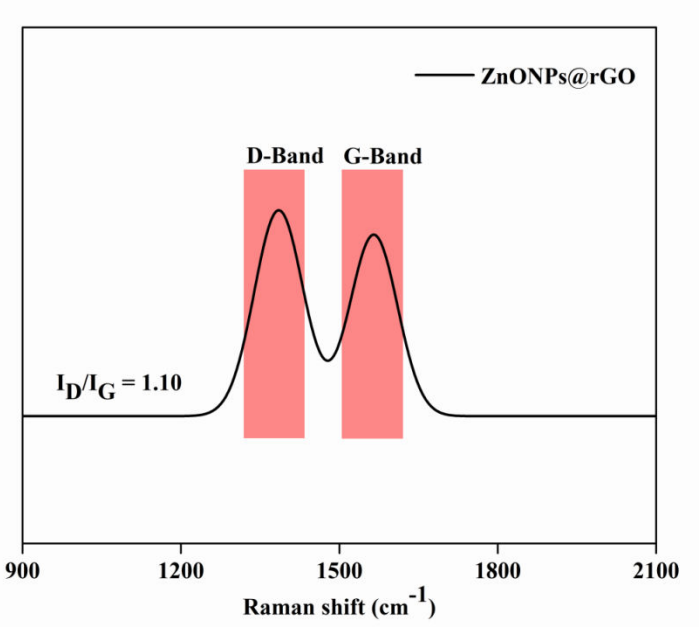

Figure 1 The Raman spectrum of ZnONPs@rGO

In view of the fact that the Raman spectroscopy is an imperative tool to construe the structure in predominantly defects and disorder nature of graphene-based materials, we have taken Raman spectrum of the synthesized compound. The Raman spectrum of ZnONPs@rGO nanocatalyst is shown in Fig. 1, which exhibits two notable peaks at around ~1383 and ~1563 cm^{-1} subsequent to the precise D- and G- band, respectively. The graphitic peak (G band) at ~1563 cm^{-1} is owing to the E_{2g} vibrational mode of the C-C bond stretching, arises due to the sp^2 carbon network of the graphene plane, whereas, the disorder peak (D band) at ~1383 cm^{-1} is due to symmetry forbidden band of the longitudinal plane phonon vibration or k-point phonons of the A_{1g} vibrational mode.[38] The intensity ratio of the D and G bands i.e. (I_D/I_G ratio) facilitates to guesstimate the defects of graphene based compounds where a higher ratio makes sure of more defects on graphene. The calculated I_D/I_G ratio of ZnONPs/rGO nanocatalyst is 1.10, which is comparable to the spectrum of GO (see Chapter 2, fig. 10). The increment in the intensity ratio was might be due to the attachment of the metal ion on the surface of GO. Furthermore, we have also calculated the crystalline size of ZnONPs@rGO nanocatalyst (i. e. La = 17.48 nm) using Tuinstra–Koenig relation. [39]

(b) X-ray diffraction study:

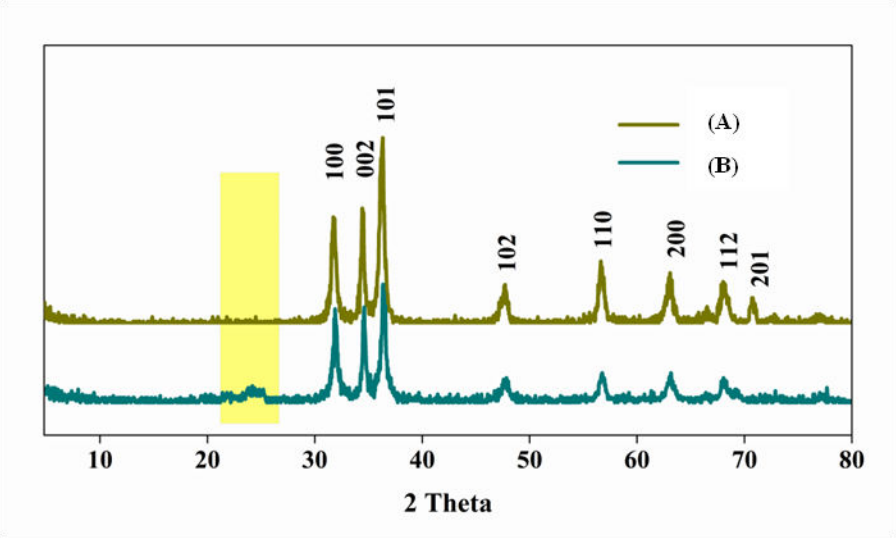

Figure 2 XRD patterns of (A) ZnONPs and (B) ZnONPs@rGO.

The XRD patterns are the prominent technique used to determine the crystallinity of as-prepared nanocatalysts. The XRD patterns of ZnONPs and ZnONPs@rGO nanocatalyst are shown in Fig. 2 whereas, XRD patterns of GO is given in Chapter 2 (see Fig. 8). The peak observed at 11.8^{o} in the XRD pattern of GO, which has been disappeared and a new diffraction peak is observed at 24.3º (Fig. 2) with inter-layered distance of 3.6 Å after the *in situ* anchoring of ZnO nanoparticles and reduction of GO nanosheets. This result clearly indicates that some of the oxygen containing debris have been abolished and the formation of new in-plane sp^2 domains during the reduction process. The aforesaid results are in well accordance with Raman and XPS results. In the XRD patterns of ZnONPs@rGO nanocatalyst [Fig. 2(B)], the diffraction peaks at 31.7º, 34.4º, 36.1º, 47.6º, 56.7º, 62.9º, 68.0º and 70.9º were reconcilable with those of (1 0 0), (0 0 2), (1 0 1), (1 0 2), (1 1 0), (1 0 3), and (1 1 2), respectively, [8] pointing towards the hexagonal wurtzite structure of ZnO (JPCDS 36-1451). These results are more uniform to that observed in neat ZnONPs XRD patterns [Fig. 2(A)]. [40] The diffraction peak observed at 24.3º, due to the distinctive absorption peak for graphene. Whereas no such peak was observed together with no strong absorption observed at the diffraction peak of 11.8º, suggesting that the GO is changed into reduced graphene oxide during the reduction process.

(c) X-ray photoelectron spectroscopy:

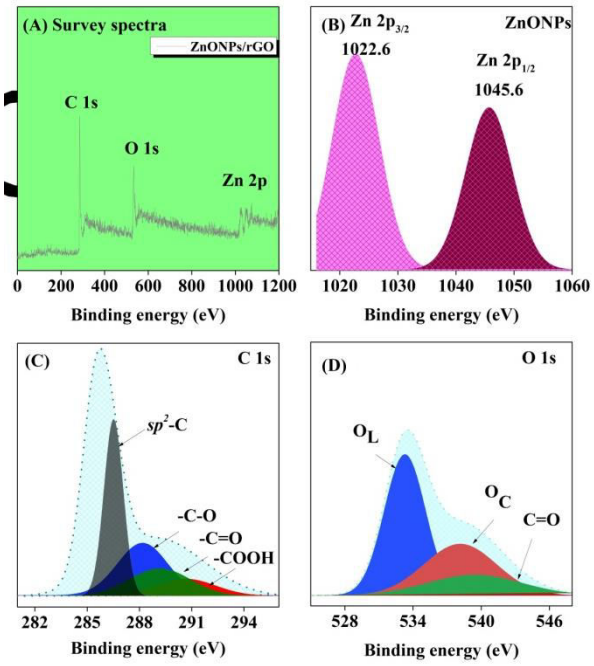

Figure 3 XPS spectra (A) survey spectra of ZnONPs@rGO, (B) Zn sp core level spectrum, (C) C 1s spectra of ZnONPs@rGO and (D) O 1s spectra of ZnONPs@rGO

The surface chemical composition and bonding environment of as-prepared nanocatalyst was analyzed by the x-ray photoelectron spectroscopy (XPS). As shown in Fig. 3(A), the survey spectra of ZnONPs@rGO are displayed three prominent elements C 1S, O 1S and Zn 2p at about 282.9, 534.8, and 1031.8, respectively. In the Zn 2p core level spectra [Fig. 3(B)], two prominent peaks observed at 1022.6 eV and 1045.6 eV corresponds to Zn $2p_{3/2}$ and Zn $2p_{1/2}$, respectively, indicating that Zn was present in the form of zinc oxide.

While comparing C 1s spectra of GO (see Chapter 2, Fig. 9) with the high-resolution C 1s spectra of ZnONPs@rGO nanocatalyst [Fig. 3(C)] four prominent peaks observed at 286.4, 288.2, 289.3 and 291.3 eV, assigned to sp^2-C, -C–O, -C=O, and -COOH, respectively. These results showed that the intensity of peaks -C–O, -C=O and -COOH was considerably low and while the magnitude of sp^2-C peak was dramatically increased owing to the restoration of the sp^2 domains in the new plane. These results are in well agreement with the Raman spectra. The high resolution O 1s spectrum of ZnONPs@rGO nanocatalyst [Fig. 3(D)] has

shown three peaks at ~533.2, ~538.2 and ~539.3 eV. Among them, the first two peaks are attributed to the lattice oxygen (O_L) and chemisorbed oxygen (O_C) species, respectively, whereas the later peak observed at ~539.3 eV, indicating the C=O bond in the wurtzite structure of hexagonal ZnO.

(d) High resolution Transmission electron microscopy (HR-TEM):

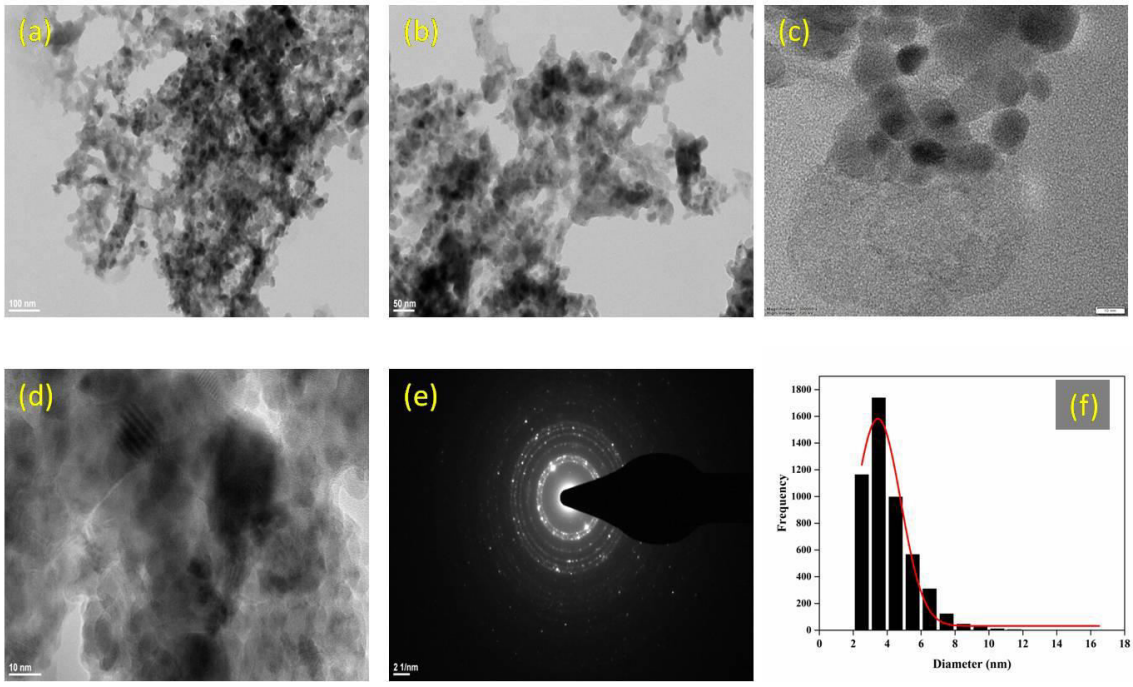

Figure 4 (a, b) Low magnification TEM image of ZnONPs@rGO, (c, d) HR-TEM image of ZnONPs@rGO with fringe spacing, (e) SAED pattern of ZnONPs@rGO, (f) Histogram graph of ZnONPs@rGO.

The HR-TEM images of ZnONPs@rGO nanocatalyst are shown in Fig. 4. The TEM images of ZnONPs/rGO demonstrated the fine narrow sized ZnO nanoparticles were dispersed on rGO nanosheet [Fig. 4 (a, b)]. The ZnO nanoparticles have observed an average particle size of 3.45±1.58 nm [Fig. 4(f)] and have clearly shown the size distribution of ZnO nanoparticles on the rGO nanosheet, which was investigated by image J software. As depicted in Fig. 4(d), the nanocatalyst has given the information pertaining to the crystal lattice fringes

of ZnONPs with a d-spacing of 0.22 nm, indicating with the plane of cubic ZnONPs. In the SAED image of ZnONPs@rGO [Fig. 4(e)], the diffraction pattern was perceived, which substantiates the polycrystalline nature of ZnONPs on the surface of rGO nanosheets. The intense spherical dots of ZnONPs were also observed in the SAED pattern. These results are in well agreement with the XRD data as discussed above.

(e) FTIR spectra

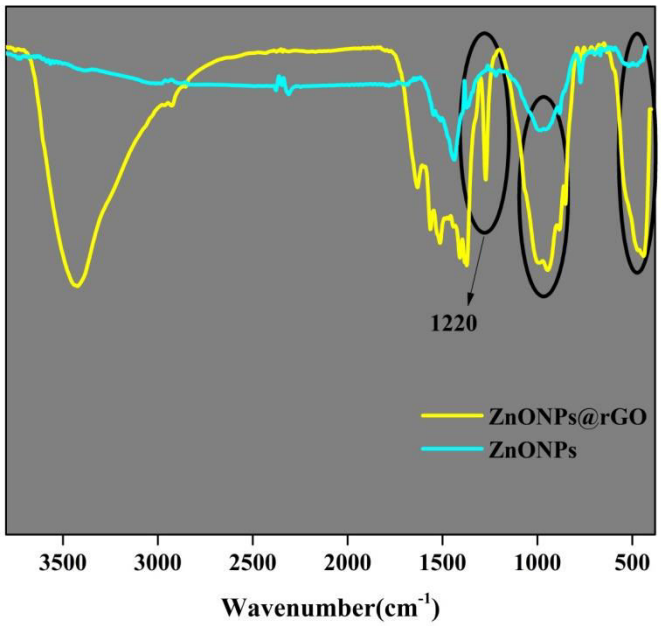

Fig. 5 FTIR spectra of ZnONPs and ZnONPs@rGO.

The FTIR spectra of ZnONPs and ZnONPs@rGO are shown in Fig. 5. In the FTIR spectrum of ZnONPs, the band observed at 496 cm^{-1}, which indicates the vibrational mode of Zn-O bonds. However, in the spectrum of ZnONPs@rGO, this band was slightly moved towards the lower wavelength (480cm^{-1}), which might be due to ZnO nanoparticle supported on rGO nanosheet [41.]. Moreover, the peak observed in the FTIR spectrum of ZnONPs at ~950 cm^{-1} is assigned to Zn-OH bonds. The same band was also seen in the FTIR spectrum of ZnONPs@rGO. In the FTIR spectrum of ZnONPs@rGO, two additional stretching vibrations are observed at ~3440 and in the region, 2860-2880 cm^{-1}, are corresponding to the -OH and aromatic C-H stretching vibrations, respectively. In the FTIR spectra of GO (Chapter 2, Fig. 6), the intense peak observed at around

1700 cm^{-1} is due to $\upsilon_{(C=O)}$ stretching vibration of the –COOH group, was disappeared in the spectra of ZnONPs@rGO. In addition to this, one prominent peak observed at 1220 cm^{-1} in the spectra of ZnONPs@rGO, is due to the epoxy group and was remained intact after the chemical reduction process. [41]

(f) Thermogravimetric study

In the subsequent section, the thermal behavior of the as-synthesized catalyst, characterized on the basis of thermogravimetric method is discussed. The quantitative purpose of the organic content and the thermal stability of the compound have been achieved through the thermogravimetric analysis. The thermogram of ZnONPs@rGO nanocatalyst is fairly matched with GO. As shown in Fig. 6, the first weight loss (~6.2%) observed in the temperature range 110-280 ºC is assigned to the removal of the most of the oxygen containing functional groups. This was followed by a gradual plunge in the weight loss of 49.6% in the temperature range of 400- 650 ^{o}C, assumed to be due to the pyrolysis of carbonaceous stuff of the graphene nanosheets.

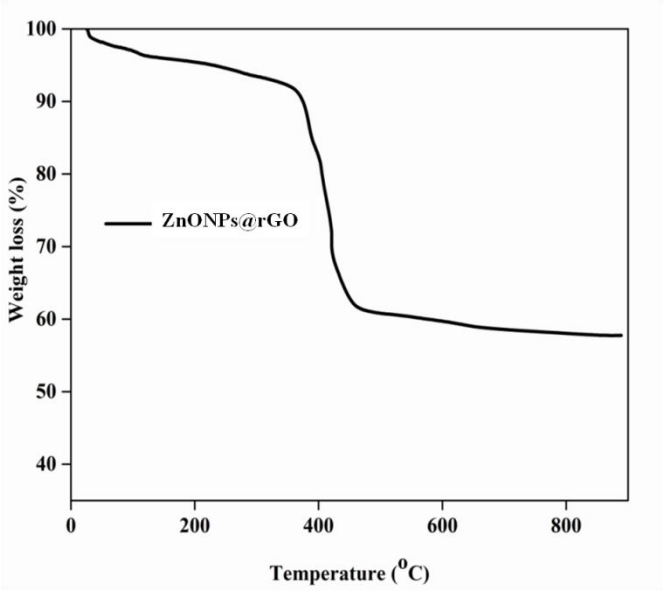

Fig. 6 TG analysis of ZnONPs@rGO.

[4.4] Catalytic study

In the previous section, as-prepared nanocatalysts have been successfully synthesized and characterized. However, herein this segment, we have discussed

the catalytic activity of as-synthesized nanocatalysts executed over the One-pot A^3-coupling reaction using aldehyde, ethyl acetoacetate and urea as starting materials and ethanol as a greener solvent to form 3,4-dihydropyrimidin-2 (1H)-ones as the main product (Scheme-1).

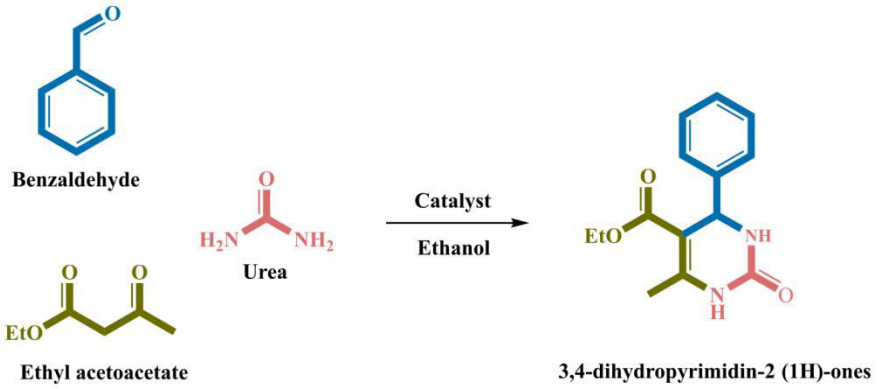

Scheme 1 A schematic representation of Biginelli reaction.

Under the typical reaction conditions, A^3-components i.e. Benzaldehyde (1 mmol), ethyl acetate (1 mmol) and urea (0.8 mmol) were dissolved into 5 mL ethanol and then 10 mg catalyst was taken in RBF. To acquire the optimum results, first, all the catalysts like GO, ZnO, CuO, ZnONPs@rGO, and CuNPs@rGO were employed to get best-suited catalyst for this Biginelli reaction and the results are shown in Fig. 7. The results clearly indicate that very minute or inferior yields are observed with species like graphite, GO, ZnO, CuO and without catalyst. However, the conspicuous results are observed with supported systems like ZnONPs@rGO and CuNPs@rGO. Amongst them, ZnONPs@rGO has found most suitable catalyst giving optimal yield (84%) under the optimized conditions and therefore, it has been chosen for further experiments.

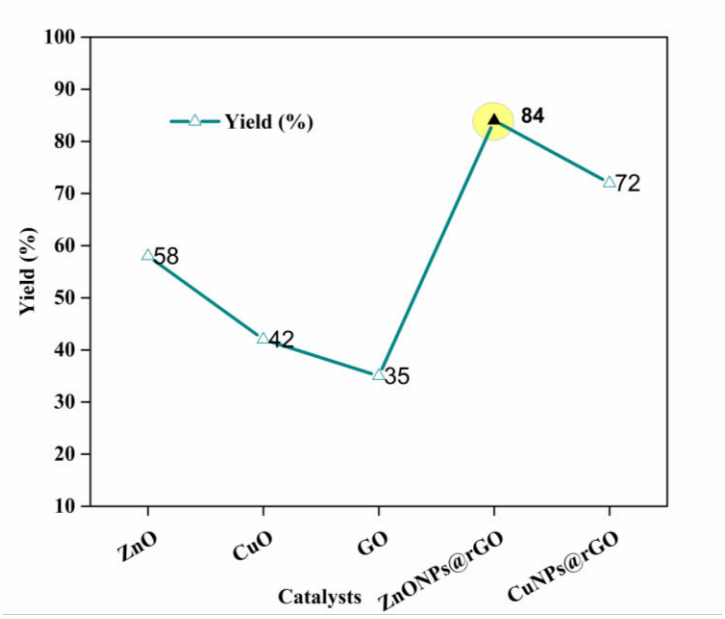

Figure 7 The catalytic activity of various catalysts for one-pot A^3-coupling reaction. Reaction conditions: benzaldehyde (1 mmol), Ethyl acetoacetate (1 mmol), Urea (0.8 mmol) varying catalysts (10 mg), Ethanol (5 mL), temp. (Reflux), Time (3.5 h)

Factor affecting the one-pot A^3-coupling reactions

(a) Effect of catalyst dosage

The catalyst concentration is a one of the significant aspects in the A^3-coupling reaction. As shown in fig. 8, five different dosages viz. 5 mg, 10 mg, 15 mg, 20 mg, and 30 mg of the representative catalyst, i.e. ZnONPs/rGO were taken with keeping all other reaction parameters fixed: temperature (65°C), benzaldehyde (1 mmol), ethyl acetoacetate (1 mmol), urea (0.8 mmol), ethanol (5 mL), and reaction time (3.5 h). The results are shown in Fig. 8. The maximum yield (93%) of the product was achieved with 15 mg of catalyst. While further increasing the catalyst amount showed a downward trend of the product yield (see Fig. 8). The reduction trend in the product yield was might be due to certain concentration of the product adsorbed on the catalytic active sites. As a result, the optimal catalyst amount has taken to be 15 mg for the further investigation.

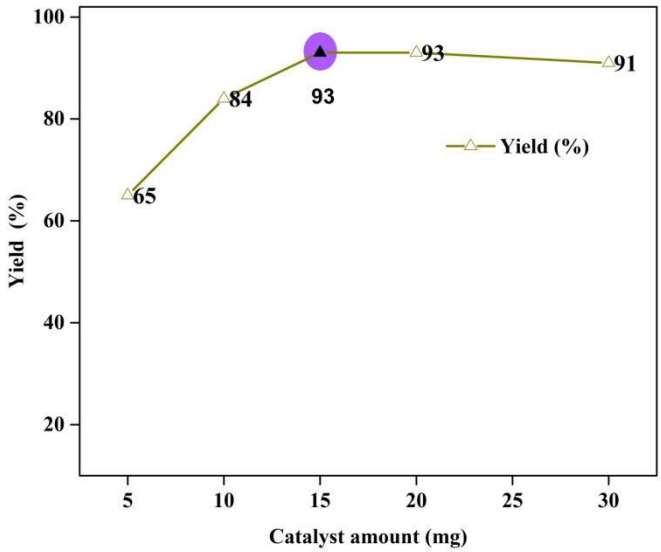

Figure 8 The effect of catalyst dosage for One-pot A^3-coupling reaction.

Reaction conditions: benzaldehyde (1 mmol), Ethyl acetoacetate (1 mmol), Urea (0.8 mmol) ZnONPs@rGO (**X** mg), Ethanol (5 mL), temp. (Reflux), Time (3.5 h).

(b) Effect of various solvents

The effect of varying solvents such as polar protic i.e. ethanol, polar aprotic i.e. acetonitrile (ACN) and non-polar i.e. toluene was examined (Fig. 9) over A^3-coupling reaction with other parameters kept fixed to increase the yield of the product. As shown in Fig. 9, the product yield achieved with different solvent systems in the decreasing order as Ethanol (93%) > ACN (75%) > toluene (51%). Initially, we have also performed the aforesaid catalytic reaction without solvent, however; as prophecy, we could not observe the as-expected elevated yield (21%). Among the various solvent systems, when ethanol was utilized, an optimum yield of the product (93%) was obtained. Consequently, ethanol is preferred to be used as a solvent for the aforesaid reaction.

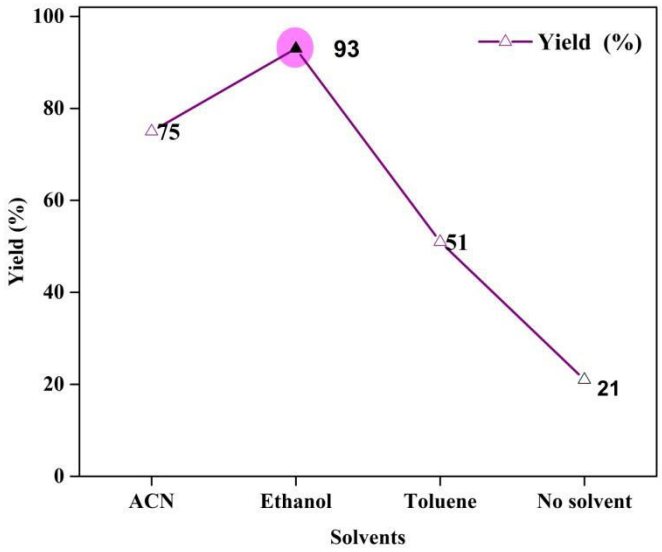

Figure 9 The effect of various solvents for One-pot A^3-coupling reaction. Reaction conditions: benzaldehyde (1 mmol), Ethyl acetoacetate (1 mmol), Urea (0.8 mmol) ZnONPs@rGO (15 mg), **various solvents** (5 mL), temp. (Reflux), Time (3.5 h).

(c) Effect of Amount of Urea

Varying amount of urea such as 1:1:0.8, 1:1:1, 1:1:1.2, and 1:1:1.4 with benzaldehyde, ethyl acetoacetate are employed to examine their effect on the A^3-coupling reaction with keeping all other parameters fixed. A key role of urea is clearly perceptible from Fig. 10. Highest product yield of 3,4-dihydropyrimidin-2 (1H)-ones (97%) is obtained with 1:1:1 mole ratio, while on further increasing the concentration of urea with increasing mole ratios i.e. 1:1:1.2 and 1:1:1.4, a downtrend is observed with product yield of 93% and 89%, respectively. This reduction was believed to be due to the probability of the extra urea and water to form ammonium. Hence, 1:1:1 mole ratio is preferred for the further experiments keeping other parameters fixed.

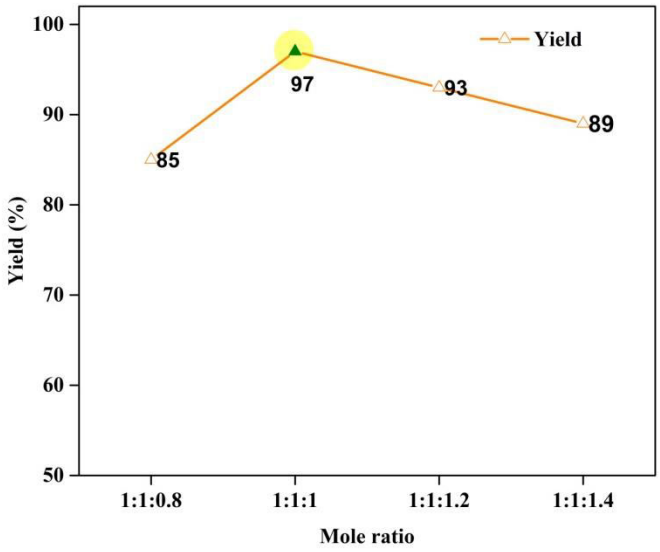

Fig. 10 The effect of various amount of urea for One-pot A^3-coupling reaction. Reaction conditions: benzaldehyde (1 mmol), Ethyl acetoacetate (1 mmol), Urea (**X** mmol) ZnONPs@rGO (15 mg), various solvents (5 mL), temp. (Reflux), Time (3.5 h).

(d) Effect of Time

To obtain the precise isolated yield of the product, it is of rather imperative to end up the reaction at accurate time. This study is aiming to find out the accurate time for this multicomponent A^3-coupling reaction using ZnONPs@rGO as a representative catalyst. As shown in Fig. 11, we have conducted this experiment at five different time viz. 1, 2, 3, 3.5 and 5 h by keeping other parameters fixed. It can be seen from the figure that to begin with at 1 h, 42% isolated product yield was attained. However, on enduring the reaction with time, the product yield also upholds in the increasing trend and achieved maximum (93%) at 3.5 h. If the reaction still continued to 5 h, no further increment in the yield of the product was achieved. As a result, we have chosen 3.5 h as the ideal time for further examination of other experimental variables.

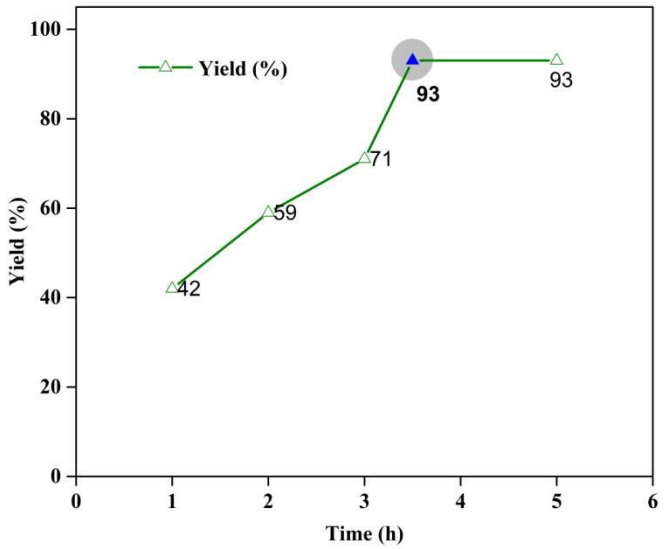

Figure 11 The effect of varying time for One-pot A^3-coupling reaction.

Reaction conditions: benzaldehyde (1 mmol), Ethyl acetoacetate (1 mmol), Urea (1 mmol) ZnONPs@rGO (15 mg), various solvents (5 mL), temp. (Reflux), Time (**X** h).

[4.5] Biginelli reaction using diverse aldehydes, β-keto esters, and urea over ZnONPs/rGO as a representative nanocatalyst

After getting the optimized conditions, we have further been exploring the scope of A^3-coupling reaction etiquette by altering substrates like aldehydes, ethyl and/or methyl acetoacetate and urea producing a wide range of dihydropyrimidinones (DHPMs) and its derivatives (Table 1). When the reactions using various aldehydes including electron withdrawing group (i.e. 4-methyl benzaldehyde and/or 4-methoxy benzaldehyde) and/or electron donating group (i.e. 4-nitrobenzaldehyde), ethyl acetoacetate and urea gave comparatively exceptional yield than the product yields acquired using various aldehydes, methyl acetoacetate and urea (Table 1). Consequently, ethyl acetoacetate is quite better substrate than methyl acetoacetate. [43]

Table 1 The scope of ZnONPs@rGO nanocatalyst over Biginelli condensation reaction using various aldehydes, β-keto esters and urea.

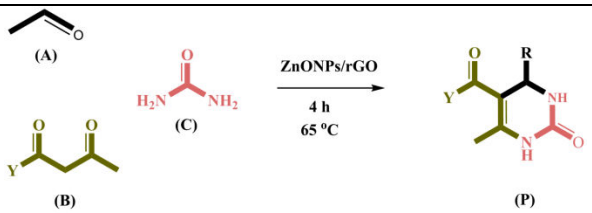

Entry	(A)	(B)	(C)	Yield (%)	Temperature (°C)	
					Found	Reported[refer.]
1	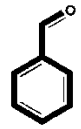	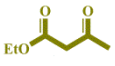		93	203-205	201-204[1]
		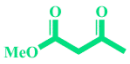		90	213-214	212-215[2]
2	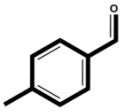	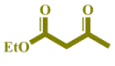		89	196-198	192-194[1]
		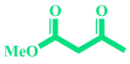	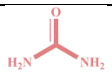	82	201-202	202-204[5]
3	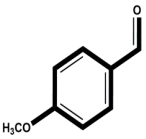	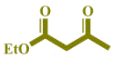		88	201-203	204-206[5]
		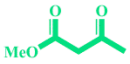		83	190-193	193-195[5]
4	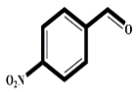	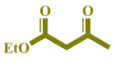	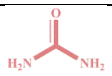	85	207-208	207-210[3]
		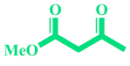		78	212-214	213-215[4]
5	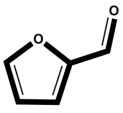	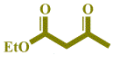	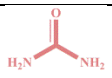	90	206-208	209-211
		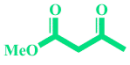		87	202-203	204-206

[4.6] The plausible reaction mechanism for Biginelli reaction using ZnONPs/rGO as a representative catalyst

A plausible mechanism for the Biginelli condensation reaction using ZnONPs@rGO as a representative catalyst is demonstrated in Scheme 2. The reaction begins with the activation of a carbonyl group via the attachment of the substrate (aromatic aldehyde) onto the active site of ZnONPs@rGO, followed by the nucleophilic attack of urea to an activated aldehyde, so as to generate the intermediate species (i.e. imine adduct). This imine intermediate is attacked by an ethyl acetoacetate molecule forming another intermediate (Scheme 2). It was then followed by the addition-elimination reactions, leading to the formation of the desired product. [43]

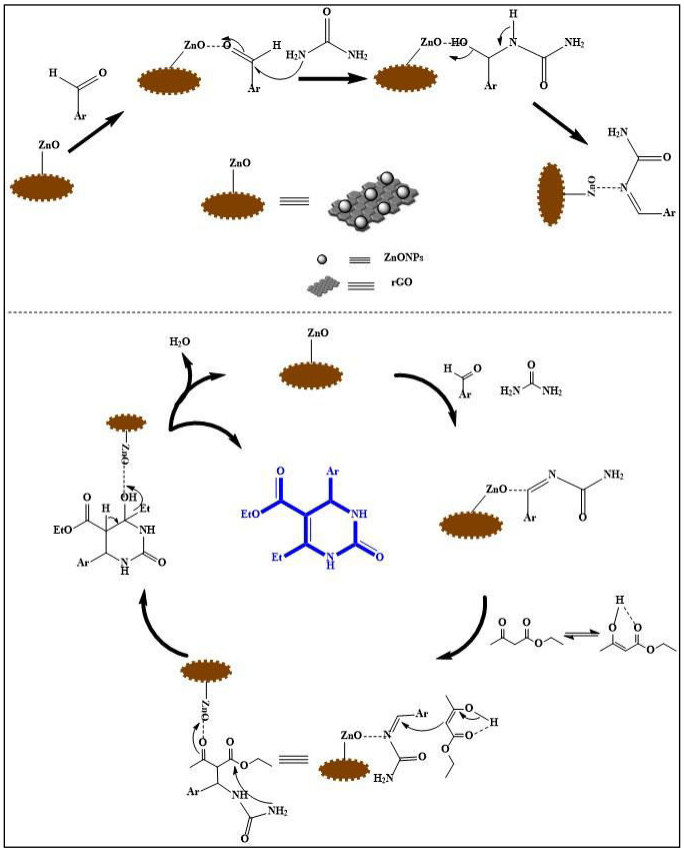

Scheme 2. A plausible reaction mechanism for the Biginelli condensation reaction over ZnONPs@rGO nanocatalyst.

[4.7] Recyclability Test

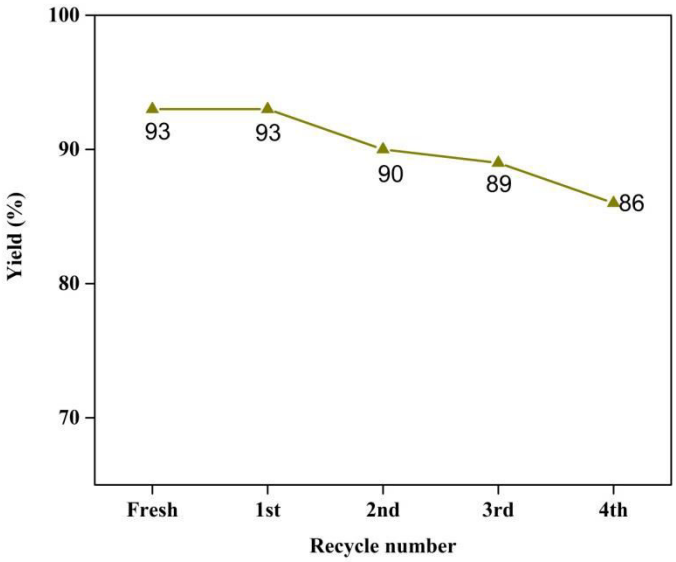

Figure 12 The recyclibility for One-pot A^3-coupling reaction.

Reaction conditions: benzaldehyde (1 mmol), Ethyl acetoacetate (1 mmol), Urea (1 mmol) ZnONPs@rGO (15 mg), various solvents (5 mL), temp. (Reflux), Time (3.5 h).

The reusability of the catalyst is of gargantuan consequence applicable to any heterogeneous catalytic system. The reusability of ZnONPs@rGO as a representative catalyst was tested over A^3-coupling reaction and the results are shown in Fig. 12. Prior to examine this, the catalyst is alienated by filtration from the reaction mixture and washed several times with acetonitrile followed by drying in an oven before utilizing for the further catalytic test. As seen in Fig. 12 it was recycled up to 5 times without any significant loss in activity, despite the fact that in the 4^{th} and 5^{th} run, the product yield decreasing up to 97.9% and 90%, respectively. [43]

[4.8] Comparison study (Table 2)

No.	Catalysts	Conditions	Time	Yield (%)	Ref.
1	Fe_3O_4@SBA-15 (0.084)	EtOH, 363 K	6	85	1
2	D-Xylonic acid	100, D-Xylonic acid	5	89	2

3	Partially Fluorinated, Water-Stable Cu(II)−MOF	60, Solvent free	2	89	3
4	PPF-SO_3H(sulfonic acid functionalized polypropylene fiber)	Reflux, Ethanol	8	74	4
5	12-Tungstophosphoric acid	Reflux, AcOH	6-7	70	5
6	$FeCl_3.6H_20$	Relux, ACN	12	88	6
7	ZnONPs@rGO	Reflux, EtOH	3.5	93	Present work

In the past couple of years, catalytic studies over A^3-coupling reaction by various research groups using diverse homogeneous and/or heterogeneous catalysts have been discussed and are tabulated in Table 2. J. Mondal et al. [44] have executed the Biginelli reaction over Fe_3O_4@SBA-15 as an efficient heterogeneous catalyst using ethanol as a solvent at 90 ^oC, achieving 85% product yield after 6 h (Table 2, entry 1). Ma J et al. [45] have accomplished Biginelli reaction over D-Xylonic acid as a catalyst, getting 89% product yield after 5 h at 100 ^oC (Table 2 entry 2). P. K. Bharadwaj et al. [46.] developed a partially fluorinated, water-stable Cu(II)−MOF catalytic system, achieving a maximum of 89% product yield at 60 ^oC after 2 h (Table 2, entry 3). XL Shi and co-workers [47] have reported the Biginelli reaction catalyzed by PPF-SO_3H (sulfonic acid functionalized polypropylene fiber) using ethanol as a solvent under reflux for 8 h, achieving 74% product yield (Table 2, entry 4). FF Bamoharram and co-workers [48] have used 12-Tungstophosphoric acid as a catalyst for Biginelli reaction under reflux for 6-7 h, achieving 70% of the product yield (Table 2, entry 5). Furthermore, $FeCl_3.6H_2O$ used as a catalyst by ZT Wang and co-workers [49] over Biginelli reaction using acetonitrile as a solvent (under 12 h reflux time), obtaining 88% of the product yield (Table 2, entry 6). Here in this thesis chapter, our own results (Table 2, entry 7) show that, when ZnONPs@rGO was used for 'one-pot' A^3-

coupling reaction under optimized reaction condition bestowed exceptional product yield of 93 % in 3.5 h under ambient temperature.

[4.9] Conclusion

In conclusion, we have synthesized and fully characterized ZnONPs@rGO nanocatalysts. The as-synthesized ZnONPs@rGO catalysts demonstrated exceptional catalytic activity for Biginelli condensation reaction to give preferred DHPM products in good to admirable yields. Moreover, the plausible catalytic mechanism for the aforesaid condensation reaction has also been proposed and discussed. The nanocatalyst ZnONPs@rGO also exhibited tremendous stability, recyclability and leaching-resistant performance with recycled up to five times without significant loss of activity.

[4.10] References

[1] (a) T. Boer, A. Amore, R.V.A. Orru, *Microwaves in Organic Synthesis Second Edition*, Wiley-VCH, Weinheim, 788 (2006).
(b) M. Malacria, *Chem. Rev*., **96**, 289 (1996).

[2] (a) C.D. Graaff, E. Ruijter, R.V.A. Orru, *Chem. Soc. Rev*. **41,** 3969 (2012),
(b) M.H. Majid, S. Asadi, B.M. Boshra, *Mol. Divers*. **17,** 389 (2013).

[3] K.S. Atwal, G.C. Rovnyak, S.D. Kimball, D.M. Floyd, S. Moreland, B.N. Swanson, J.Z. Gougoutas, J. Schwartz, K.M. Smillie, M.F. Malley, *J. Med. Chem*. **33,** 2629 (1990).

[4] (a) T.M. Mayer, T.M. Kapoor, S.J. Haggarty, R.W. King, S.L. Schreiber, T.J. Mitchison, *Science,* **286,** 971 (1999);
(b) C.O. Kappe, O.V. Shishkin, G. Uray, P. Verdino, *Tetrahedron*, **56**, 1859 (2000).

[5] C.O. Kappe, *Acc. Chem. Res*. **33,** 879 (2000).

[6] L. Heys, C.G. Moore, P.J. Murphy, *Chem. Soc. Rev*. **29,** 57 (2000).

[7] D. Astruc, F. Chardac, *Chem. Rev.* **101**, 2991 (2001).

[8] B. Helms, JMJ Fréchet, *Adv. Synth. Catal*. **348**, 1125 (2006).

[9] M. Shema-Mizrachi, G. M. Pavan, E. Levin, A. Danani, N. G. Lemcoff, *J. Am. Chem. Soc*. **133**:14359 (2011).

[10] E. L. Margelefsky, R. K. Zeidan, M. E. Davis, *Chem. Soc. Rev.* **37**, 1118 (2008).

[11] A. Mondoli, M. Lessi, D. Pini, C. Evangelisti, P. Salvadori, *Adv. Synth. Catal.* **350**, 375 (2008).

[12] K. Ding, Z. Wang, L. Shi, *Pure Appl. Chem*. **79,** 1531 (2007).

[13] Z. Wang, G. Chen, K. Ding, Chem. Rev. **109**, 322 (2009)

[14] L. Marchetti, M. Levine, *ACS Catal.* **1**, 1090 (2011).

[15] Z. Zhang, Z. Wang, *J. Org. Chem.,* **71**, 7485 (2006).

[16] S. B. Kim, P. D. Pike, D. A. Sweigart, *Acc. Chem. Res.* **46**, 2485 (2013).

[17] B. M. Choudhary, R. M. Sharma, K. K. Rao, *Tetrahedron,* **48**, 719 (1992).

[18] L. Djakovitch, M. Wagner, C. G. Hartung, M. Beller, K. Kohler, *J. Mol. Catal. A* **219**, 121 (2004).

[19] L. Yin, J. Liebscher, *Chem Rev,* **107**, 133 (2007).

[20] N. Pal, A. Bhaumik, *RSC Adv*, **5**, 24363 (2015)

[21] Y.-B. Huang, J. Liang, X.-S. Wang, R. Cao, *Chem. Soc. Rev.*, **46**, 126 (2017).

[22] H. Li, Q. Pan, Y. Ma, X. Guan, M. Xue, Q. Fang, Y. Yan, V. Valtchev, S. Qiu, *J. Am. Chem. Soc.,* , **138**, 14783 (2016).

[23] H. Wang, C. Wang, Y. Yang, M. Zhao, Y. Wang, *Catal. Sci. Technol*., **7**, 405 (2017).

[24] H. Li, J. He, A. Riisager, S. Saravanamurugan, B. Song, S. Yang, *ACS Catal*., **6**, 7722 (2016).

[25] J. Du, M. Tao, W. Zhang, *ACS Sustainable Chem. Eng*., **4**, 4296 (2016).

[26] D. Bhuyan, M. Saikia, L. Saikia, Catal. Comm., **58**, 158 (2015).

[27] X. Huo, J. Liu, B. Wang, H. Zhang, Z. Yang, X. She, P. Xi, *J. Mater. Chem. A*, **1**, 651 (2013)

[28] D. Elhamifara, D. Elhamifarc, F. Shojaeipoor, J Mole. Catal. A Chemi. **426**, 198 (2017).

[29] Y. Chen, Z. Hu, Y. Chang, H. Wang, Z. Zhang, Y. Yang, H. Wu, *J. Phys. Chem. C*, **115**, 2563 (2011).

[30] B. Li, H. Cao, *J. Mater. Chem*.**, 21**, 3346 (2011).

[31] K. S. Shin, H. Jo, H.-J. Shin, W. M. Choi, J.-Y. Choi, S.-W. Kim, *J. Mater. Chem.*, **22**, 13032 (2012).

[32] A. Kumar, D. Saxena, M. Gupta, *Green Chem*., **15**, 2699 (2013).

[33] P. Ghosh, A. Das, *J. Org. Chem*. **78**, 6170 (2013).

[34] U. Rajesh, J. Wang, S. Prescott, T. Tsuzuki, D. Rawat, *ACS Sustainable Chem. Eng.*, **3**, 9 (2015).

[35] Z. Li, H. Zhao, H. Han, Y. Liu, J. Song, W. Huo, W. Chu, Z Sun, *Tetrahedron Letters* **58**, 3984 (2017).

[36] Q. Zhang, C. G. Tian, A. P. Wu, et al. *J. Mater. Chem.* **22**, 11778 (2012).

[37] R. Vithalani, D. Patel, C. K. Modi, N. N. Som, P. K. Jha, S. R. Kane, *Diamond Relat. Mater.,* **90**, 154 (2018).

[38] S. Mondal, S. Sudhu, S. Bhattacharya, S. K. Saha, *J. Phys. Chem. C*, **119**, 27749 (2015).

[39] F.Tuinstra, J. L. Koenig, *J. Chem. Phys*., **53**, 1126 (1970).

[40] S. Yang, X. Feng, S. Ivanovici, K. Muellen, *Angew. Chem. Int. Ed.*, **49**, 8408 (2010).

[41] K. B. Babitha, J. Jani Matilda, A. Peer Mohamed, S. Ananthakumar, *RSC Adv.*, **5**, 50223 (2015).

[42] D. Bhuyan, M. Saikia, L. Saikia, Micro. Meso. Mater. **256**, 39 (2018).

[43] Z. Ghadamyari, A. Shiri, A. Khojastehnezhad, S. Mohammad Seyedi, *Appl Organometal Chem*. 5091 (2019).

[44] J. Mondal, T. Sen, A. Bhaumik, *Dalton Trans*. **41**, 6173 (2012).

[45] J. Ma, L. Zhong, X. Peng, R.Sun, Green Chem. **18**, 1738 (2016).

[46] T. K. Pal, D. De, S. Senthilkumar, S. Neogi, P. K. Bharadwaj, *Inorg. Chem*. **55**, 7835 (2016).

[47] X. L. Shi, H. Yang, M. Tao, W. Zhang, *RSC Adv*. **3**, 3939 (2013).

[48] M. M. Heravi, F. Derikvand, F. F. Bamoharram, *J. Mol. Catal. A* **242**, 173 (2005).

[49] Z. T. Wang, L. W. Xu, C. G. Xia, H. Q. Wang *Tetrahedron Letters*. **45**, 7951 (2004).